Dalton Transactions

Accepted Manuscript

ROYAL SOCIETY OF CHEMISTRY

www.rsc.org/dalton

Journal Name

RSCPublishing

ARTICLE

Thiophene-based terpyridine and its zinc halide complexes：Synthesis, crystal structures and third-order nonlinear optical properties in near-infrared region

Cite this: DOI: 10.1039/x0xx00000x

Jingyun Tan,†[a] Rui Li,†[a] Dandan Li, [a] Qiong Zhang, [a] Shengli Li,[a] Hongping Zhou,[a] Jiaxiang Yang, [a] Jieying Wu,[a,*] Yupeng Tian[a,b,*]

Received 00th September 2014,
Accepted 00th October 2014

DOI: 10.1039/x0xx00000x

www.rsc.org/dalton

A novel 4'-(4-(diphenylamino)thienyl)-2,2':6',2''-terpyridine ligand (**L**) based on thiophene and its $\mathbf{LZnX_2}$ complexes (X=Cl, Br, I, SCN) were designed, synthesized and characterized by elemental analysis, Far-IR, MALDI-TOF-MS, and single crystal X-ray diffraction analysis. The structural studies revealed that the central zinc (II) atom adopted a distorted trigonal bipyramidal coordination model. However, there were different hydrogen bonds and stacking models with different counter anions in the crystals. The absorption properties of the compounds were investigated with aiding of TD-DFT computational methods. Furthermore, the third-order nonlinear optical (NLO) properties were systematically studied *via* open-aperture Z-scan methods using tunable wavelength femtosecond laser. The results from photophysical property investigations suggested that the complexation of the thiophene-based terpyridine ligand with zinc halides resulted in strong ICT/LLCT bands about 450 nm, and the complexes exhibited strong nonlinear optical response in the near-infrared range around 850 nm. Above all, the two-photon absorption (2PA) cross-section values (σ) was enhanced by the coordination with zinc and influenced by halide ions, reaching up to 2583 GM (X=Br).

Introduction

Nonlinear optics (NLO) is the branch of optics that describes the behavior of light in media where the dielectric polarization responds nonlinearly to (the electric field component of) light.[1, 2] Recently, materials with remarkable NLO properties in near-infrared (NIR) region have been extensively exploited due to their numerous potential applications in optical communication, optical data processing and storage, three-dimensional microfabrication, frequency-upconversion lasing, optical power limiting and bioimaging.[3-7]

So far as we know, the push–pull π-conjugated system might possesses the main and most promising foundation for NLO materials.[8,9] There are two basic kinds of push–pull models, donor-acceptor (D-A) and donor-π-chromophore-acceptor (D-π-A) constructions. It is known that extending of conjugated system to construct novel large D-π-A molecule contributes positive impact on the enhancement of NLO response. However, the compounds with large conjugated system are normally thermally unstable and synthetic processes are time consuming,[10] which limited their various practical applications. Moreover, recent studies suggested that a large π-conjugated organic ligand may result in decreasing NLO effect while coordinated with metal ions, which was opposite to the original intention.[11-13] Therefore, economically designing as smaller molecule as possible while with stronger NLO effect for practical applications gradually appear as a novel conception.[14,15]

Compared with inorganic, organic and polymeric materials, metal complexes can well combine the merits as follows:[16-19] 1) More sublevels in the energy hierarchy, which permit more allowed electronic transition to take place and resulting a larger NLO effect; 2) High damage threshold and fast response, which are important factors for their practical applications. Consequently, considerable attentions have been paid to the complexes with NLO effect nowadays.

The complexes of 2,2′:6,2″-terpyridine derivatives have aroused widespread concern and great interest for their distinguished photophysical and electrochemical properties. In combine with transition metal ions, 2,2′:6,2″-terpyridines form

distorted configuration complexes showing different stabilities from kinetically inert to labile (e.g., Zn(II)).[20-22] The attainable and the low cost of zinc show a considerable advantage compared with the other potential metals. In particular, when Zn(II) binds to terpyridine with conjugated aryl substituents, an efficient intramolecular charge transfer (ICT) from the substituted aryl donor (D) to the metalated terpyridine acceptor (A) takes place upon light excitation.[23,24]

Further more, thiophene derivatives have attracted much attention due to the rich electronic feature of the thiophene moiety.[25-28] Thiophene unit acts as a π-conjugated bridge, which owns higher stability than double bond, and higher electron delocalization than benzene. Therefore, it can be used to construct molecular optoelectronic functional materials. It was proposed that the derivatives containing thiophene unit should result in large molecular hyperpolarizability and charge transfer, which are necessary for NLO responses.[29,30]

Considering above, here we first rationally synthesized a novel ligand 4'-(4-(diphenyl- amino)thienyl)-2,2':6', 2''-terpyridine (**L**) and its Zn(II) complexes (**$LZnCl_2$**, **$LZnBr_2$**, **$LZnI_2$** and **$LZn(SCN)_2$**) (Scheme 1). Specifically, this design was based on the following considerations: 1) **L** with D-A construction combines the electron rich property of diphenylamine (as D) with the electron-withdrawing ability of terpyridine (as A), which can strongly bind towards metal ions; 2) Distinct bathochromic-shift of their absorption properties could be expected after introducing thiophene ring as both donor and bridge into a π-conjugated system; 3) Zn(II) within the complexes can arouse stronger charge transfer;[31,32] 4) As a systematic work, the influences on their structures and photophysical properties should be investigated for the four halide ions (Cl, Br, I and SCN) in the complexes.

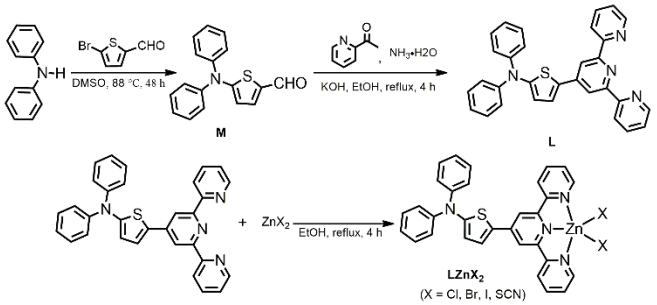

Scheme 1 Synthetic route for ligand **L** and complexes **$LZnCl_2$, $LZnBr_2$, $LZnI_2$ and $LZn(SCN)_2$**

Experimental

Measurements and Methods

All chemicals were commercially available and all solvents were purified by conventional methods before use.

Elemental analyses were performed with a Perkin Elmer 240C elemental analyzer. The ^{1}H NMR spectra were recorded at 25 °C on a Bruker Avance 400 spectrometer, and the chemical shift are reported as parts per million from TMS (δ). Coupling constants J are given in Hertz. Mass spectra were acquired on a Micromass GCT-MS (EI source). Fourier transform infrared spectra (FT-IR) were recorded on a NEXUS-870 (Nicolet) spectrophotometer in the 4000-50 cm^{-1} region (mid-IR: 4000-400 cm^{-1}, using a powder sample on a KBr plate; far-IR: 600-50 cm^{-1}, using a powder sample on a PE film attached with paroline. UV-vis absorption spectra were recorded on a UV-265 spectrophotometer. Fluorescence measurements were carried out on a Hitachi F-7000 fluorescence spectrophotometer. NLO properties were measured by the Z-scan technique with a femtosecond laser pulse and Ti: 95 Sapphire System (680~1080 nm, 80 MHz, 140 fs, Chameleon II) as the light source. The beam was spatially filtered to remove higher-order modes and tightly focused using a 5 cm focal length lens. The incident average power of 100 mW was adjusted by a Glan prism. The thermal heating of the sample with high repetition rate laser pulse was removed by the use of a mechanical chopper running at 10 Hz. A 1 mm cell of the sample in DMF at 1.0×10^{-3} $mol\cdot L^{-1}$ was put in the light path, and all measurements were carried out at room temperature.

Crystallography

The X-ray diffraction measurements were performed on a Bruker SMART CCD area detector using graphite monochromated Mo-K_α radiation (λ = 0.71069 Å) at 298(2)K. Intensity data were collected in the variable ω-scan mode. The structures were solved by direct methods and difference Fourier syntheses. The non-hydrogen atoms were refined anisotropically and hydrogen atoms were introduced geometrically. Calculations were performed with SHELXTL-97 program package.[33]

TD-DFT studies

Optimizations were carried out with B3LYP/6-311+G(d,p) and B3LYP[LANL2DZ] without any symmetry restraint. All calculations, including optimizations and TD-DFT, were performed with the G03 software.[34] Geometry optimization of the singlet ground state and the TD-DFT calculation of the lowest 25 singlet-singlet excitation energies were calculated with a basis set composed of 6-311+G(d,p) for C, H, N, O and S atoms and the Lanl2dz basis set for the Zn, Cl, Br and I atoms. The basis set was downloaded from the EMSL basis set library. The lowest 25-spin allowed singlet-singlet transitions, up to energy of about 5 eV, were taken into account for the calculation of the absorption spectra.

Synthetic procedures

Synthetic route for ligand **L** and complexes **$LZnCl_2$, $LZnBr_2$, $LZnI_2$ and $LZn(SCN)_2$** were shown in Scheme 1.

Synthesis of compound M. Phenanthroline (0.45 g, 2.3 mmol), cuprous iodide (0.46 g, 2.4 mmol), anhydrous potassium carbonate (5.00 g, 36 mmol) and diphenylamine (1.86 g, 11 mmol) were placed in an oven-dried 250 mL Schlenk flask. The reaction vessel was evacuated and filled with high purified argon, a process which was repeated three times. Then refined dimethylsulfoxide (120 mL) and 5-bromo-2-thiophene carbaldehyde (1.90 g, 10 mmol) were added with a syringe under a counter-flow of argon. At last, 18-Crown-6 (0.04 g, 0.15 mmol) and Aliquat-336 (0.02 g, 0.05 mmol) were added. The reaction was stirred at 88 °C for 48 h. Upon completion of the reaction, the mixture was cooled to room temperature. The mixture was filtered through a Buchner funnel to remove the deposition, then diluted with water (500 mL) and stirred for 24 h. A yellowish-brown product was obtained after the separation of water by a Buchner funnel again. Purification of the residue by column chromatography on silica gel (Petroleum ether / Ethyl acetate 20:1) gave **M** as yellow powder, 1.37 g, with yield of 49%. M. p. = 97 °C. ^{1}H-NMR (d_6-acetone, 400 MHz, ppm): δ= 6.39 (d, J= 4.4Hz, 1H), 7.29 (t, J= 10.0Hz, 2H), 7.35 (d, J= 8.0Hz, 4H), 7.46 (q, J= 8.0 & 10.0Hz, 4H), 7.66 (d, J= 4.4Hz, 1H), 9.64 (s, 1H). ^{13}C-NMR (d_6-DMSO, 150 MHz): δ= 125.59, 126.58, 127.94, 129.46, 130.03,

139.53, 145.46, 163.29, 182.19. IR (KBr, cm^{-1}): 3087 (w), 3039 (w), 2805 (m), 2760 (m), 1889 (w), 1663 (vs), 1580 sm), 1524 (m), 1485 (s), 1424 (s), 1386 (s), 1349 (s), 1220 (m), 755 (m), 691 (m). Calcd. for $C_{17}H_{13}NOS$(279.36): C, 73.09; H, 4.69; N, 5.01%. Found: C, 73.13; H, 4.71; N, 5.03%. MALDI-TOF: *m/z*, *cal*: 279.07, found: 279.26 $[M^+]$.

Synthesis of ligand L. In 80 mL ethanol solution, **M** (2.80 g, 10 mmol) was added, stirring at room temperature, then 2.70 g (22 mmol) 2-acetylpyridine and KOH (2.90 g, 50 mmol) which was dissolved with water as little as possible, were added successively. After 10 min, ammonia (25%, 62 mL, 400 mmol) was added by 3 portions. The reaction was stirred at 85 °C for 4 h. The mixture were cooled to room temperature and filtered, giving **L** as yellow solid, with yield of 1.95 g, 40%. M.p. = 198 °C. ^{1}H NMR (d_6-DMSO, 400 MHz, ppm) δ = 8.73 (d, 2H), 8.62 (d, 2H), 8.50 (s, 2H), 8.01 (t, 2H), 7.77 (d, 1H), 7.51 (t, 2H), 7.41 (t, 4H), 7.20(m, 6H), 6.66 (d, 1H). ^{13}C NMR (101 MHz, d_6-$CDCl_3$) δ = 156.0, 154.1, 149.1, 147.5, 143.7, 136.8, 133.5, 129.4, 125.1, 123.8, 123.48 (s), 121.3, 119.5, 116.1. IR (KBr, cm^{-1}): 3035 (m), 1610 (m), 1581(s), 1463 (s), 1008 (s), 790 (s), 694 (s).Far-IR (cm^{-1}):516(vw), 504(vw), 400(vw). Anal. Calcd. for $C_{31}H_{22}N_4S$(482.60): C, 75.15; H, 4.59; N, 11.61 %. Found: C, 75.18; H, 4.63; N, 11.59 %. MALDI-TOF: *m/z*, *cal*: 482.16, *found*: 481.98 $[M^+]$.

Synthesis of complex $LZnCl_2$. A solution of **L** (0.2413 g, 0.5 mmol) in dichloromethane/methanol (10mL/30 mL) was mixed with a zinc chloride (0.0681 g, 0.5 mmol) in methanol (10 mL) and the reaction mixture was refluxing for 4 h. The mixture were cooled to room temperature and filtered, giving $LZnCl_2$ as yellowish-brown solid with yield of 0.27 g, 90%. M.p. > 350 °C. ^{1}H NMR (d_6-DMSO, 400 MHz, ppm) δ= 8.85 (d, 2H), 8.81 (s, 2H), 8.69 (s, 2H), 8.27 (t, 2H), 8.21 (s, 1H), 7.84 (s, 2H), 7.45(t, 4H), 7.26 (m, 6H), 6.67 (s, 1H); IR (KBr, cm^{-1}): 3059 (m), 1604(s), 1543(m), 1473(s), 1438 (vs), 1376 (m), 1019(s), 792 (m), 698 (m), 512(m). Far-IR(cm^{-1}):512(s), 504(m), 478(m), 437(m), 411(s), 364(w), 301(s), 276(m). Anal. Calcd. for $C_{31}H_{22}Cl_2N_4SZn$ (618.88): C, 60.16; H, 3.58; N, 9.05%; found: C, 60.20; H, 3.59; N, 9.07%. MALDI-TOF: *m/z*, *cal*: 616.02, *found*: 580.51 $[M\text{-}Cl]^+$.

A similar synthesis procedures were also adopted for the other complexes $LZnBr_2$, $LZnI_2$ and $LZn(SCN)_2$.

Synthesis of complex $LZnBr_2$. Yellowish-brown solid with yield of 0.31 g, 90%. M.p. > 350 °C. ^{1}H NMR (d_6-DMSO, 400 MHz, ppm) δ = 8.88 (m, 4H), 8.72 (s, 2H), 8.33 (t, 2H), 8.22 (d, 1H),7.89 (t, 2H), 7.45 (t, 4H), 7.28(m, 6H), 6.68 (d, 1H). IR (KBr, cm^{-1}): 3058 (m), 1607(m), 1572(m), 1542(m), 1473(s), 1437 (vs), 1376 (m), 1020(m), 792 (m), 699 (m), 512(m). Far-IR(cm^{-1}):513(s), 503(m), 477(m), 437(m), 411(s), 364(w), 224(s), 203(m). Anal. Calcd. for $C_{31}H_{22}Br_2N_4SZn$ (707.79): C, 52.61; H, 3.13; N, 7.92%; found: C, 52.62; H, 3.16; N, 7.95%. MALDI-TOF: *m/z*, *cal*: 703.92, *found*: 625.05 $[M\text{-}Br]^+$.

Synthesis of complex $LZnI_2$. Red solid with yield of 0.36 g, 90%. M.p.> 350 °C. ^{1}H NMR (d_6-DMSO, 400 MHz, ppm) δ= 8.96 (d, 2H), 8.89 (s, 2H), 8.75 (s, 2H), 8.37 (t, 2H), 8.24 (s, 1H), 7.93 (t, 2H), 7.46 (t, 4H), 7.28 (m, 6H), 6.71 (s, 1H); IR (KBr, cm^{-1}): 3046 (m), 1600(m), 1536(m), 1432 (vs), 1373 (m), 1015(m), 786 (m), 693 (m), 512 (m). Far-IR(cm^{-1}):515(s), 499(m), 477(m), 444(m), 410(s), 355(m), 205(s), 189(m). Anal. Calcd. for $C_{31}H_{22}I_2N_4SZn$ (801.79): C, 46.44; H, 2.77; N, 6.99%; found: C, 46.46; H, 2.80; N, 6.98%. MALDI-TOF: *m/z*, *cal*: 799.89, *found*: 672.98$[M\text{-}I]^+$.

Synthesis of complex $LZn(SCN)_2$. Orange-Red solid with yield of 0.30 g, 90%. M.p.= 330 °C. ^{1}H NMR (d_6-DMSO, 400 MHz, ppm) δ= 8.96 (s, 2H), 8.80 (s, 2H), 8.74 (s, 2H), 8.38 (t, 2H), 8.24 (s, 1H), 7.94 (s, 2H), 7.45 (m, 4H), 7.28 (m, 6H), 6.73 (s, 1H); IR (KBr, cm^{-1}): 3056 (m), 2083(s), 1601(m), 1536(m), 1433 (vs), 1374 (m), 1017(m), 788 (m), 695 (m), 516 (m). Far-IR(cm^{-1}):518(s), 508(m), 481(m), 449(m), 409(s), 351(w), 280(s), 254(m). Anal. Calcd. for $C_{33}H_{22}N_6S_3Zn$ (664.14): C, 59.68; H, 3.34; N, 12.65%; found: C, 59.66; H, 3.35; N, 12.68%. MALDI-TOF: *m/z*, *cal*: 662.04, *found*: 603.67 $[M\text{-}(SCN)]^+$.

Results and discussion

Crystallography

The single crystals of **L**, $LZnCl_2$, $LZnI_2$ and $LZn(SCN)_2$, suitable for the X-ray diffraction analysis, were obtained from acetonitrile at room temperature. Unfortunately, for many times, the solvent evaporation method, solvent diffusion method and solvothermal technique had been tried but failed to obtain a suitable single crystal (always been filamentary) of $LZnBr_2$. In contrast, the shape of $LZnCl_2$, $LZnI_2$ and $LZn(SCN)_2$ was needle-like, granular and rhombus, respectively. The tiny structural difference may lead to various process of single crystal growth, and in this way $LZnBr_2$ tended to form filamentary crystal which cannot been detected at present.

The structures are shown in Fig. 1. The crystal data collection and refinement parameters are given in Table 1. The selected bond distances and angles are summarized in Table 2. The geometrical parameters of the hydrogen bonds are listed in Table 3. The hydrogen bonds and stacking modes of **L**, $LZnCl_2$, $LZnI_2$ and $LZn(SCN)_2$ are shown in Fig. 2 and Fig. 3, respectively.

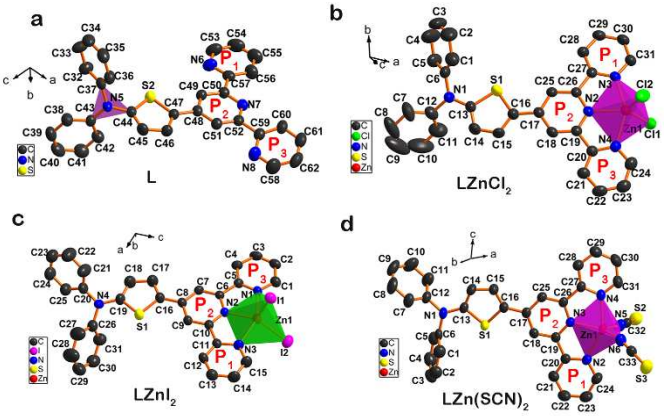

Fig. 1 Structures and coordination patterns of **L**, $LZnCl_2$, $LZnI_2$ and $LZn(SCN)_2$; H atoms are omitted for clarity; Thermal ellipsoids are drawn at 50% probability.

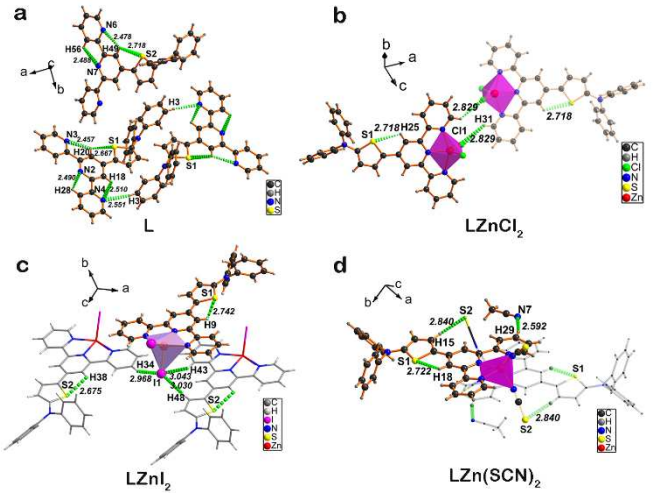

Fig. 2 Hydrogen bonds of **L, LZnCl$_2$, LZnI$_2$** and **LZn(SCN)$_2$** (green dash bonds)

Crystal Structure of L. This crystal belongs to monoclinic system with P2$_1$/n space group. An asymmetric unit of **L** contains two molecules (Fig. S1). With regard to the triarylamine moiety, the three rings constitute a structure like propeller, and dihedral angle between two benzene rings is 64.9°, while the dihedral angles of the two benzene and thiophene rings are 83.5° and 81.4°, respectively. The nitrogen atom adopts a trigonal-planar geometry ($\sum_{C-N-C}$ = 119.4° + 118.2° + 121.1° = 358.7°). Because of the intramolecular C–H···S hydrogen bonds (Fig. 2a), the bridge thiophene ring is almost coplanar with the terpyridine group, whose dihedral angle with the core pyridine (**P$_2$**) of terpyridine is 11.9° (Fig. S2). Compared with **L**, the dihedral angle between the bridge benzene ring and the core pyridine of terpyridine group within an analogue molecule 4'-(4-N,N-diphenylaminophenyl)- 2,2':6',2''-terpyridine[35] (labeled as **TL** in this article) is 32.7°, which is much larger. Inspection of **L** (Fig. S2), the tricentered hydrogen bond[36] C20–H20···(N3 & S1) could be responsible for the excellent planarity. **P$_2$** forms dihedral angles of 1.4° and 4.7° with **P$_3$** and **P$_1$**, respectively. There are two kinds of hydrogen bonds in the crystal, which result in two different stacking patterns (Fig. S3, Table S2).

Table 1 Crystal data and structure refinement for **L, LZnCl$_2$, LZnI$_2$ and LZn(SCN)$_2$**

Comp	**L**	**LZnCl$_2$**	**LZnI$_2$**	**LZn(SCN)$_2$**
CCDC No.	1016302	1016304	1016305	1016306
Empirical formula	$C_{31}H_{22}N_4S$	$C_{31}H_{22}N_4SCl_2Zn$	$C_{33}H_{25}I_2N_5SZn$	$C_{35}H_{22}N_7S_3Zn$
Formula weight	482.59	618.86	842.81	702.15
Temperature	298(2) K	298(2) K	291(2) K	298(2) K
Wavelength	0.71069 Å	0.71069 Å	0.71073 Å	0.71069 Å
space group	$P2_1/n$	$P\bar{1}$	$P\bar{1}$	$P\bar{1}$
Crystal system	monoclinic	triclinic	triclinic	triclinic
a/Å	13.288(5)	11.166(5)	13.682(6)	11.489(5)
b/Å	40.706(5)	11.250(5)	15.253(7)	12.260(5)
c/Å	9.100(5)	12.045(5)	18.373(9)	12.884(5)
α/(°)	90.000	95.908(5)	103.092(6)	86.754(5)
β/(°)	95.255(5)	91.729(5)	99.474(6)	66.599(5)
γ/(°)	90.000	111.298(5)	113.806(6)	84.488(5)
V/Å^3	4902(3)	1398.5(11)	3273(3)	1657.5(12)
Z	8	2	4	2
D_c/Mg m^{-3}	1.308	1.470	1.710	1.407
μ/mm^{-1}	0.160	1.172	2.731	0.966
F(000)	2016	632	1640	718
Final R indices [I>2σ(I)]	R_1 = 0.0561, wR_2 = 0.1387	R_1 = 0.0459, wR_2 = 0.1222	R_1 =0.0478, wR_2 = 0.1189	R_1 = 0.0382, wR_2 = 0.1097
Goodness-of-fit on F^2	0.907	0.909	1.004	0.993

Crystal Structure of LZnCl$_2$. Complex **LZnCl$_2$** crystallizes in triclinic system with $P\bar{1}$ space group. As shown in Fig. 1b, the metal center adopts a distorted trigonal bipyramidal N_3Cl_2 coordination, and the angles are listed as follows: [N(2)-Zn(1)-Cl(1), 123.7°; N(2)-Zn(1)-Cl(2), 117.2°; N(2)-Zn(1)-N(3), 74.4°; Cl(2)-Zn(1)-Cl(1), 119.1°; N(3)-Zn(1)-Cl(1), 96.7°; N(3)-Zn(1)-Cl(2), 100.0°]. The lengths of three Zn-N bonds are different due to unequal repulsion which formed in the progress of two-dimensional structure. The zinc atom is closer to the core pyridine ring than the other two rings, which is comparable with the case of other zinc terpyridine complexes,[37] and the bond lengths are listed as follows: [N(2)-Zn(1): 2.098 Å, N(3)-Zn(1): 2.189 Å, N(4)-Zn(1): 2.206 Å]. The distances between two chloride and zinc ions are 2.273 Å and 2.249 Å, respectively. Compared to the ligand **L**, the dihedral angle between the thiophene ring and **P$_2$** is much smaller in the complex **LZnCl$_2$**, which is 5.9° (Fig. S2c). Among the terpyridine group the dihedral angles of **P$_1$** and **P$_3$** with the core ring **P$_2$** is 6.8° and 4.4° for the complex **LZnCl$_2$**, respectively, which are slightly larger than those angles of **L** for lacking C–H···N hydrogen bonds. The non-classical hydrogen bond and π-π stacking interactions lead to three-dimensional supramolecular structure of **LZnCl$_2$**, as shown in Fig. S4**.** It was also observed from Fig. S4b and S4c, one-dimensional chain structure along *b*-axis and staircase structure along *a*-axis could be found and further two-dimensional structure formed jointly. The chain structure was generated *via* intermolecular C–H···Cl hydrogen bonds, offset face-to-face and edge-to-face π-π stacking interactions, and the staircase structure *via* intermolecular C–H···Cl hydrogen bonds (Fig. S4a). Through weak edge-to-face π-π stacking interactions, layered three-dimensional structure was formed along the *c*-axis (Fig. S4d). More details were shown in Fig. S4.

Crystal Structure of LZnI$_2$. Generally, complex **LZnI$_2$** owns the similar structural features with **LZnCl$_2$**. For instance, **LZnI$_2$** also crystallizes in triclinic system with $P\bar{1}$ space group and Zn(II) also adopts a distorted trigonal bipyramidal N_3Cl_2 coordination. However, the difference is that one asymmetric unit of **LZnI$_2$** contains two target molecules and two acetonitrile molecules (Fig. S1). The two target molecules are parallel and anti-aligned. The bond lengths of Zn-I in **LZnI$_2$** [I(3)-Zn(2), 2.590Å; I(4)-Zn(2), 2.621Å] are longer than Zn-Cl in **LZnCl$_2$** (2.273 Å and 2.249 Å). In addition, the angles of I(3)-Zn(2)-I(4) is 115.7°, which is smaller than Cl(2)-Zn(1)-

Cl(1) in **LZnCl$_2$** (119.1°). The dihedral angles between **P$_1$** and **P$_3$** with the core ring **P$_2$** are 2.4° and 2.9°, respectively. Those structural features show that there is a higher degree of electron delocalization in the **LZnI$_2$** complex. As shown in Fig. 2c and Table S2, because of larger ionic radius and higher polarization than chloride ion, there are abundant intermolecular C–H···I hydrogen bonds between one iodide ion and another **LZnI$_2$** molecule, which cause a different stacking pattern compared with **LZnCl$_2$** (Fig. 3c). The compact three-dimensional structure of **LZnI$_2$** also benefit from the extensive existence of offset face-to-face π-π stacking interactions (Fig. S5e). More details were shown in Fig. S5.

Crystal Structure of LZn(SCN)$_2$. Thiocyanate ion belongs to pseudo-halogen, thus the structure of complex **LZn(SCN)$_2$** should be similar with the former two complexes mentioned. The differences should be given as follows. Due to a smaller steric hindrance, N atom from SCN coordinates with zinc ion to form a shorter bond [N(5)-Zn(1), 1.979 Å; N(6)-Zn(1), 1.950 Å] than N atoms from terpyridine. Another characteristic should be noted that the core zinc ion does not line up with the three atoms of the thiocyanate group, forming an angle of 168.9° and 161.3°, respectively (Fig. 1d). The thiocyanate groups stretch like two long arms, which permit the terminal electron-rich sulfur atoms to form weak interactions with the other molecules. In the case of **LZn(SCN)$_2$**, intermolecular C–H···S hydrogen bonds and non-covalent S···S weak interactions could be found, which lead to new stacking pattern (Fig. S3d). It is noteworthy that π-π stacking interactions were found neither in one-dimensional structure nor in two-dimensional structure. The reason could also be given that the linear type thiocyanate acted as long support fixing molecules remotely. The three-dimensional structure is formed *via* weak edge-to-face π-π stacking interactions along *b*-axis, and the stereoscopic diagram was shown in Fig. S6e. More details were shown in Fig. S6.

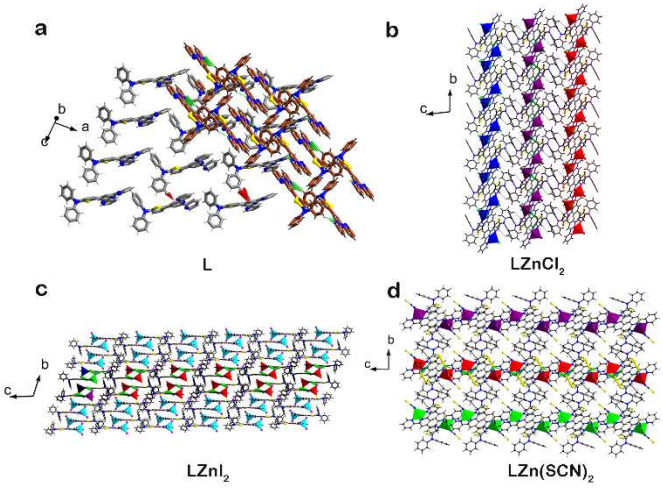

Fig. 3 Stacking modes of a) **L** viewing from *b*-axis, b) **LZnCl$_2$** viewing from *a*-axis, c) **LZnI$_2$** viewing from *a*-axis and d) **LZn(SCN)$_2$** viewing from *a*-axis

On the whole, **L** owns a rigid and preferable plane structure, which may cause the delocalization of the lone pair of electrons into the π-system. However, the stacking of **L** is loose. The complexation with zinc halide improves the compactness, as well as the planarity of the framework. Different halide ions lead to various intermolecular interactions in the crystals, and eventually to different stacking patterns.

Melting point analysis

The melting point of **L** is 198 °C, while complex **LZnCl$_2$**, **LZnBr$_2$**, **LZnI$_2$**, and **LZn(SCN)$_2$** are all exceed 300 °C. It is obviously that the coordination of **L** with zinc ion enhance the thermostability. With regard to the four complex, the melting point of **LZn(SCN)$_2$** is 330 °C, while the other are all exceed 350 °C. The difference could be explained by the deficiency of π-π stacking interactions in the structure of **LZn(SCN)$_2$**.

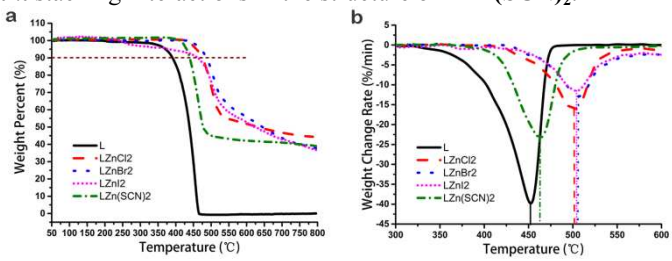

Fig. 4 TG diagrams (a) and DTG diagrams (b) of L, $LZnCl_2$, $LZnBr_2$, $LZnI_2$ and $LZn(SCN)_2$

Thermogravimetric properties

Thermal decomposition behavior of **L, LZnCl$_2$, LZnBr$_2$, LZnI$_2$** and **LZn(SCN)$_2$** were studied by thermogravimetry (TG) and derivative thermogravimetry (DTG) methods in the temperature range 20–800 °C in a flowing atmosphere of nitrogen gas. The TG and DTG curves were presented in Fig. 4, and showed one mass loss stage for any material. The decomposition temperature (10 wt% loss) of **L, LZnCl$_2$, LZnBr$_2$, LZnI$_2$** and **LZn(SCN)$_2$** is 390 °C, 473 °C, 486 °C, 460 °C and 438 °C, respectively. At 464 °C, **L** was almostly vanished, while **LZnCl$_2$, LZnBr$_2$, LZnI$_2$** and **LZn(SCN)$_2$** shown mass loss of about 6.8%, 3.4%, 11.0% and 38.7%, respectively. As shown in Fig. 4b, T_p (the maximum weight loss rate) of **L, LZnCl$_2$, LZnBr$_2$, LZnI$_2$** and **LZn(SCN)$_2$** is 452 °C, 501 °C, 506 °C, 503 °C and 464 °C, respectively. In short, the thermal stability of all the four complexes exceed the ligand largely, and among them, **LZnBr$_2$** behave the best.

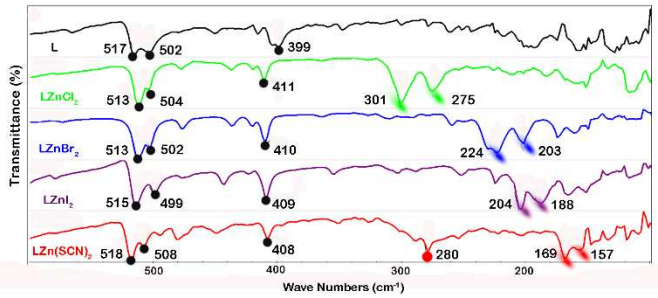

Fig. 5 Far IR spectra of **L**, **LZnCl$_2$**, **LZnBr$_2$**, **LZnI$_2$** and **LZn(SCN)$_2$**

Far-IR Spectra[38]

As shown in Fig. 5, the bands around 515 cm^{-1} and 400 cm^{-1} are shared by **L** and its complexes **LZnCl$_2$**, **LZnBr$_2$**, **LZnI$_2$** and **LZn(SCN)$_2$**, which could be considered as the in-plane ring deformation and out-of-plane ring deformation, respectively.

The out-of-plane ring deformation shifts to higher frequency after the coordination of **L** with Zn(II): 399 cm^{-1} for **L**, 411 cm^{-1} for **$LZnCl_2$**, 410 cm^{-1} for **$LZnBr_2$**, 409 cm^{-1} for **$LZnI_2$** and 408 cm^{-1} for **$LZn(SCN)_2$**. Two novel ν(Zn-X) bands(C_{2v} symmetry) are expected in the lower wave numbers range (green oblique spots for **$LZnCl_2$**, blue oblique spots for **$LZnBr_2$** and purple oblique spots for **$LZnI_2$**), which gradually shift to lower frequencies in the order of **$LZnCl_2$**, **$LZnBr_2$** and **$LZnI_2$**. Those features are in accord with crystal data mentioned above: Cl(1)-Zn(1), 2.273 Å; Cl(2)-Zn(1), 2.249 Å; I(3)-Zn(2), 2.590 Å; I(4)-Zn(2), 2.621 Å. The ν(Zn-N) bands of four complexes are inconspicuous for overlapping with fingerprint region except **$LZn(SCN)_2$**. 169 cm^{-1} and 157 cm^{-1} band could be assigned as the stretching vibration of two Zn-NCS bonds [N(5)-Zn(1),1.979 Å; N(6)-Zn(1), 1.950 Å]. In contrast, the three other ν(Zn-$N_{pyridine}$) are located in lower frequency region(fingerprint region), whose bond lengths are slightly longer than Zn-N_{NCS}. The band around 280 cm^{-1} could be assigned as δ(SCN).

Table 2 Experimental (in benzene) and calculated linear absorption properties (nm), excitation energy (eV, oscillator strengths and major contribution for **L, $LZnCl_2$, $LZnI_2$ and $LZn(SCN)_2$**.

Cmpds	Experimental data	Calculated data				
	λ_{max}(nm) / $\varepsilon(\times 10^4)$	λ_{max} (nm)	E(eV)	*f*	Composition	Character
L	390 (2.51)	413	3.00	0.1689	126→127 (H→L)	ICT($\pi_{dpa}\rightarrow\pi^*_{tpy}$)
	280 (4.21)	284	4.36	0.2724	126→133 (H→L+6)	$\pi_{dpa}\rightarrow\pi^*_{dpa}$
$LZnCl_2$	441 (2.50)	468	2.64	0.5779	139→140 (H→L)	LLCT/ICT
	327 (2.37)	329	3.76	0.1235	132→140 (H-7→L)	ICT($\pi_{tpy}\rightarrow\pi^*_{thio}$)
	315 (2.51)	307	4.04	0.1293	131→140 (H-8→L)	ICT($\pi_{dpa}\rightarrow\pi^*_{tpy}$)
$LZnBr_2$	446 (3.06)	473	2.62	0.5673	136→140 (H-3→L)	LLCT/ICT
	329 (1.81)	330	3.76	0.1301	132→140 (H-7→L)	ICT($\pi_{tpy}\rightarrow\pi^*_{thio}$)
	316 (2.01)	309	4.01	0.1199	131→140 (H-8→L)	ICT($\pi_{dpa}\rightarrow\pi^*_{tpy}$)
$LZnI_2$	448 (3.13)	485	2.55	0.3262	135→140 (H-4→L)	LLCT/ICT
	329 (2.34)	341	3.63	0.0914	135→142 (H-4→L+2)	LLCT/ICT
	317 (2.58)	317	3.91	0.0776	134→143 (H-5→L+3)	LLCT
$LZn(SCN)_2$	455 (3.54)	485	2.55	0.6281	157→162 (H-4→L)	LLCT/ICT
	329 (2.17)	331	3.75	0.0915	156→162 (H-5→L)	ICT($\pi_{tpy}\rightarrow\pi^*_{thio}$)
	318 (2.35	315	3.92	0.0826	155→162 (H-6→L)	ICT($\pi_{dpa}\rightarrow\pi^*_{tpy}$)

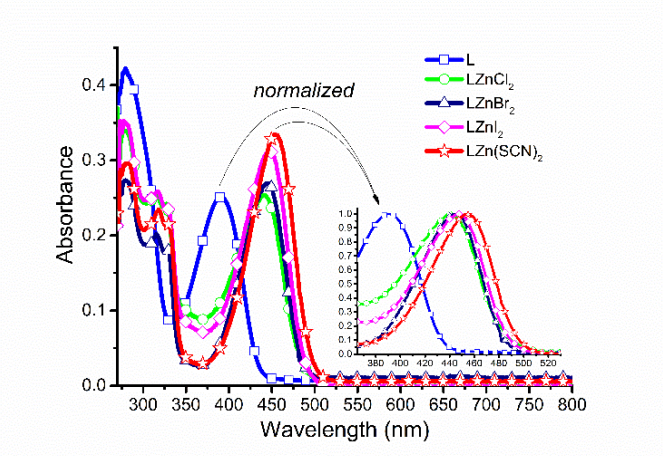

Fig. 6 UV-vis spectra of **L**, **$LZnCl_2$**, **$LZnBr_2$**, **$LZnI_2$** and **$LZn(SCN)_2$** in benzene (1.0×10^{-5} mol/L); the insert shows the normalized curves of the longer wavelength band of five molecules

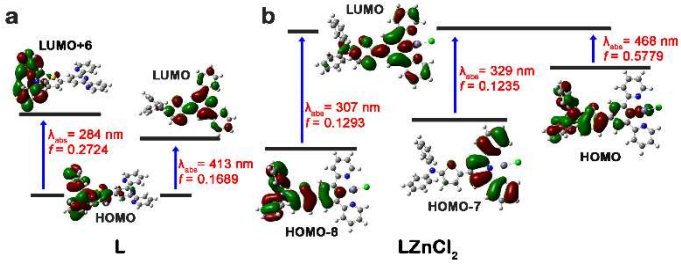

Fig. 7 Molecular orbital energy diagram for **L** and **$LZnCl_2$** (TD-DFT/b3lyp)

Linear absorption and TD-DFT studies

The absorbance data of **L, $LZnCl_2$, $LZnBr_2$, $LZnI_2$** and **$LZn(SCN)_2$** ($c=1.0\times10^{-5}$ mol/L) in different solvents were summarized in Fig. S7, Table S3.

The linear absorption spectrum of **L** in benzene is shown in Fig. 6, from which one can see that its absorption spectrum exhibits dual bands in the 270-400 nm range. The low-energy band was tentatively assigned to intraligand charge transfer (ICT) transition. Because the ε and wavelength of this band was ~25100 and ~390 nm, respectively, which meet the features of ICT transition. Likewise the high-energy band (280 nm, ε = 42100 $L\cdot mol^{-1}\cdot cm^{-1}$) was assigned to the π-π* transition of the triarylamine moiety.[31] As shown in Fig. S7, a weak solvatochromism was observed, indicating the **L** molecule with fairly small dipole moment and the difference in dipoles

between ground and excited state. By contrast, the low-energy band of **TL** is 355 nm,[31] namely the ICT transition bands of **L** show a stronger bathochromic shift effect. This can be interpreted that the thiophene ring is more electron-rich moiety than benzene ring, thus increase the electron delocalization in the π-conjugated system and lower the energy of **L**. On the other hand, the better planarity of **L**, as detailed above, also makes it easier for electron to migrate in the π-conjugated system.

Herein, as an illustration for the spectra of the complexes, the case of **$LZnCl_2$** will be described in detail. Three main bands could be found from the Fig. S7b. The intense absorption at ~280 nm(ε = 33600 $L\cdot mol^{-1}\cdot cm^{-1}$, in benzene) originates from the π-π* transition of the triarylamine moiety, which is in accord with the ligand **L**. The second band locates at ~320 nm and appears as doublet (ε = 25100 $L\cdot mol^{-1}\cdot cm^{-1}$, 23700 $L\cdot mol^{-1}\cdot cm^{-1}$) with a gap of about 10 nm, which could also be assigned to ICT transition. The last strongest band has red shift exceed 50 nm compared with **L**, and appears around 450 nm with molar absorption coefficient all exceeding 20000 $L\cdot mol^{-1}\cdot cm^{-1}$. Compared with large π-conjugated organic ligand the halide ions was rarely regarded as important moiety in recent discussion for charge transfer of metal complex. Indeed, we thought that the influences of halide ions cannot be ignored in a certain aspect. Thus the LLCT transition between the vice-ligand X (X = Cl) and the main ligand and ICT transition should be responsible for this low-energy band absorption.[39-41] The similar spectral profiles of the other three complexes can also be found (Fig. S7). Based on the experimental results, it can be proposed that the absorption spectra of the complexes display red-shift in the order of **$LZnCl_2$, $LZnBr_2$, $LZnI_2$** and **$LZn(SCN)_2$**. The reasons are presented as follows: 1) The orderly increased polarizability of Cl, Br and I lower the energy of the whole molecule at correspondingly level; 2) The SCN groups further enlarge the electron delocalization region within the complex molecule.

TD-DFT computational studies are performed to further elucidate the electronic structures of the ground state of **L**, **$LZnCl_2$**, **$LZnBr_2$**, **$LZnI_2$** and **$LZn(SCN)_2$**. The schematic representation of the molecular orbitals of **L**, **$LZnCl_2$**, **$LZnBr_2$**, **$LZnI_2$** and **$LZn(SCN)_2$** are exhibited in Fig. 7 and Fig. S8, the energies and compositions of some frontier orbitals are listed in Table 2.

The band originating from HOMO→LUMO for **L** calculated intense at 413 nm is assigned to intramolecular charge transfer (ICT) transition, while at shorter wavelength (calculated at 284 nm) mainly originates from π→π* transitions of HOMO-1 to LUMO. Particularly, we found charge transfer from thiophene ring to diphenylamine moiety could also be responsible for the high energy band due to the high polarizability and electron-rich property of thiophene (Fig.7a), which could not been found by literature yet. Compared with **L**, all the four complexes show three new absorption bands. The lowest energy bands were calculated at 468 nm, 473 nm, 485 nm and 485 nm of **$LZnCl_2$, $LZnBr_2$, $LZnI_2$** and **$LZn(SCN)_2$**, respectively. These bands can be assigned to an typical ICT transition mixed a LLCT transition due to the vice-ligand X (X = Cl, Br, I) characteristic HOMO and 2,2':6',2"-terpyridine characteristic LUMO for **$LZnCl_2$, $LZnBr_2$, $LZnI_2$** and **$LZn(SCN)_2$**. The higher energy bands of **$LZnCl_2$** were calculated at 307 nm and 329 nm (transitions correspond to the HOMO-8→LUMO and HOMO-7→LUMO, respectively), which can be assigned to charge transfer transition from terpyridine to thiophene and charge transfer transition from diphenylamine moiety to terpyridine through thiophene bridge, respectively. While the complexes **$LZnBr_2$** and **$LZn(SCN)_2$** showed the same features with **$LZnCl_2$**, **$LZnI_2$** should be assigned differently, which had not been distinguished in the experiment section. From ***crystallography*** section, the angle of I-Zn-I is smaller than that of Cl-Zn-Cl, despite the fact that the radius of iodine is larger than chlorine. That odd observation is consistent with the evident connection of the electron cloud of iodine atom with zinc center. From Fig S8b and Table 2, the iodine atom showed more participation in the charge transfer than chlorine atom, bromine atom and thiocyanate group. Therefore, it can be concluded that the theoretical calculation basically agreed with the experimental results, and clearly exhibited the charge transfer more objectively.

To sum up, the thiophene moiety is key joint, which act as both favourable bridge and electron-rich donor. The complexation with Zn(II) lower the energy gap between the HOMO and LUMO of the organic moiety, which increase the probability of electrons transition. As vice-ligand, the halide ions further enlarge the conjugated system and introduce a LLCT transition. Moreover, the **$LZnI_2$** showed charge transfer differ with the other complexes, which might impact the properties diversely in some way.

Table 3 Open aperture Z-Scan measurement data for the third-order nonlinear optical parameters of **$LZnCl_2$, $LZnBr_2$, $LZnI_2$ and $LZn(SCN)_2$**

Compounds	λ_{max} (nm)	β(cm/GW)	σ(cm^4s/photon)
$LZnCl_2$	850	0.0603	2343.01
$LZnBr_2$	850	0.0665	2583.32
$LZnI_2$	850	0.0234	906.78
$LZn(SCN)_2$	850	0.0457	1774.85

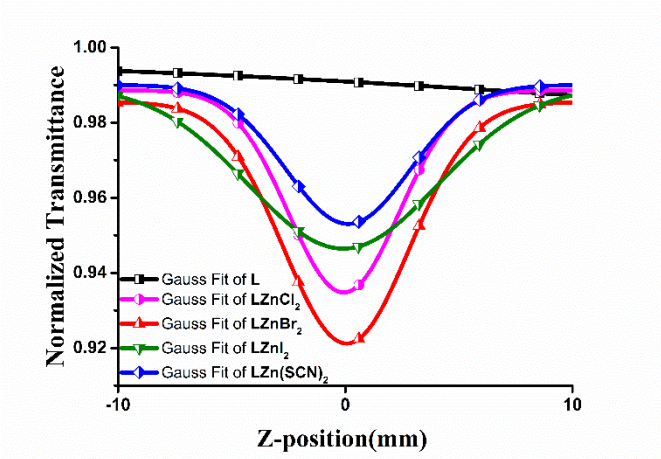

Fig. 8 Theoretical curves of a representative open-aperture Z-scan traces at wavelengths corresponding to maximum nonlinear absorption for **L**, **$LZnCl_2$**, **$LZnBr_2$**, **$LZnI_2$** and **$LZn(SCN)_2$** at 850 nm.

Nonlinear optical properties

The NLO properties of **L**, **$LZnCl_2$, $LZnBr_2$, $LZnI_2$** and **$LZn(SCN)_2$**) were measured by the OA (open-aperture) Z-scan technique using a tunable femtosecond laser system. Examples of OA Z-scan traces for solutions of complexes **L**, **$LZnCl_2$, $LZnBr_2$, $LZnI_2$** and **$LZn(SCN)_2$**) are shown in Fig. 8 and Fig. S9. The NLO response for all the compounds depends on the

laser wavelength, for **L**, **$LZnCl_2$**, **$LZnBr_2$**, **$LZnI_2$** and **$LZn(SCN)_2$**) the most pronounced nonlinear absorption and refraction effects were detected in the range from 680 to 1080 nm.

The NLO absorption components were evaluated by Z-scan experiment under an open-aperture configuration. The 2PA coefficient β and 2PA cross-sections (σ) were determined by the OA Z-scan technique. The theoretical data were fitted using the following equations:

$$T(z,s=1)=\sum_{m=0}^{\infty}\frac{[-q_0(z)]^m}{(m+1)^{3/2}} \quad \text{for } |q_0|<1 \qquad (1)$$

$$q_0(z)=\frac{\beta I_0 L_{eff}}{1+\chi^2} \qquad (2)$$

β is the nonlinear absorption (2PA) coefficient of the solution, I_0 is the input intensity of laser beam at focus (z = 0) divided by $\pi\omega_0^2$, L_{eff} = [1-exp(-$\alpha_0 L$)]/α_0 is the effective length with α_0 the linear absorption coefficient and L the sample length. $\chi = z/z_0$, $z_0 = \pi\omega_0^2/\lambda$ is the diffraction length of the beam with ω_0 the spot size at focus, λ is the wavelength of the beam and z is the sample position. So the nonlinear 2PA coefficient β (in units of cm/GW) can be deduced. Furthermore, the σ could be determined by the following relationship:

$$\sigma = h\gamma\beta \Big/ N_A d \times 10^{-3} \qquad (3)$$

Here, h is the Planck constant, γ is the frequency of incident laser, σ is molecular 2PA cross-section, N_A is the Avogadro number, and d is the concentration (in units of mol·L^{-1}). Based on equation (3), the molecular 2PA cross-section σ can be calculated.

From the linear absorption spectra (Fig. 6), no absorption was observed from 600 to 800 nm range, suggesting low-intensity loss and little temperature change caused by photon absorption when light propagates in the materials. This demonstrates that the NLO responses of complexes **L**, **$LZnCl_2$**, **$LZnBr_2$**, **$LZnI_2$** and **$LZn(SCN)_2$** in DMF are neat without the interference of the other absorption at the wavelength of 680-900 nm femtosecond laser by the Z-scan technique. In Fig. 8, the open-aperture transmittance was symmetric with respect to the focus (z=0). The obvious minimum transmittance unambiguously indicated a biggish nonlinear absorption which was attributed to 2PA effect.

Table 3 shows clearly that **$LZnCl_2$**, **$LZnBr_2$**, **$LZnI_2$** and **$LZn(SCN)_2$** exhibit a discernible two-photon absorption values with a maximum corresponding to $\sigma \approx 2343$, 2583, 907 and 1775 GM (Goeppert-Mayer units) at 850 nm, respectively. Such a difference must be due to varied negative ion, which indicates that anions own different electro-negativity may considerably influence on the 2PA cross sections. The results show that the influences of electron inductive effect of different halide ions on the two-photon absorption properties (Br>Cl>SCN>I) differ with those on the linear absorption properties as mentioned before (SCN>I>Br>Cl). This significant decrease of two-photon absorption value of **$LZnI_2$** could be ascribed to the heavy atom effect (HAE) of iodine atom. Moreover, as P. N. Prasad declared,[5] there was a strong correlation between intramolecular charge-transfer processes and two-photon absorptivity from the viewpoint of electronic structures and photophysical processes. The TD-DFT studies showed the charge transfer of **$LZnI_2$** is distinctive indeed, namely, the large polarizability of iodine actually influence the two-photon absorptivity somehow. To date, the influence of halogen atoms on the NLO properties remain undefined.[42-44]

Those kinds of contradictions indicated that as to a push-pull system, the linear and nonlinear properties obey different laws, namely, the matching level of orbital energy has various influence on the behaviors of a material.

These relative high values suggest that the zinc-based complexes as near-IR nonlinear optical materials can lead to potential applications in future.

Conclusions

A novel thiophene-based **L** and its four Zn(II) complexes **$LZnCl_2$**, **$LZnBr_2$**, **$LZnI_2$** and **$LZn(SCN)_2$**, were synthesized. Their structures were confirmed crystallographically. It was found that the four terpyridine zinc halide complexes adopted a distorted trigonal bipyramidal N_3Cl_2 coordination, and various intermolecular interactions caused by different halide ions eventually lead to different stacking patterns. The thermogravimetry experiments demonstrated that **$LZnBr_2$** shown the best thermostability. The linear absorption properties of **L** and the four complexes have been investigated combining experimental results with TD-DFT calculation methods, and the correlations between the structures and properties had been discussed in detail. The formation of Zn–N coordination bonds caused strong LLCT band and generated red-shift up to 50 nm compared with their free ligand **L**. The halide ions functioned differently on the enlargement of the π-conjugated system, following the order of SCN>I>Br>Cl. The third-order nonlinear optical properties were studied *via* open aperture Z-scan method. The complexes exhibited satisfactory two-photon absorption in the near-infrared range around 850 nm, and 2PA cross-section order were **$LZnBr_2$ > $LZnCl_2$ > $LZn(SCN)_2$ > $LZnI_2$**.

In conclusion, the complexation with zinc ion not only improved its thermostability, but also considerably enhanced the nonlinear optical response in the NIR region. It suggested that these thiophene-based complexes were proposed as new NIR NLO materials. Further endeavor for the structure-nonlinear property relationships and application optimization is ongoing in our laboratory.

Acknowledgements

This work was supported by a grant for the National Natural Science Foundation of China (21271004, 51372003, 51432001, 21271003), the Natural Science Foundation of Anhui Province (1308085MB24), Ministry of Education Funded Projects Focus on returned overseas scholar, Department of Education of Anhui Province (KJ2012A025), Program for New Century Excellent Talents in University (China), Doctoral Program Foundation of Ministry of Education of China (20113401110004).

Supporting Information Available: †Crystallographic date reported in this paper has been deposited with the Cambridge Crystallographic Date Center and allocated the deposition numbers CCDC 1016302, 1016304, 1016305, 1016306. Copies of these information may be obtained free of charge from the Director, CCDC, 12 Union Road, Cambridge CB2 1EZ, UK (fax: +44-1223/336-033; e-mail: deposit@ccdc.cam.ac.uk). Synthetic procedures and detailed experimental information; X-ray crystallographic data (CIF); computation studies; optical measurements; these information are available free of charge via the Internet at http://pubs.rsc.org.

*To whom correspondence should be addressed. E-mail: yptian@ahu.edu.cn.
a Department of Chemistry, Key Laboratory of Functional Inorganic Materials Chemistry of Anhui Province, Anhui University, Hefei 230039, P. R. China E-mail: yptian@ahu.edu.cn; jywu1957@163.com
b State Key Laboratory of Coordination Chemistry, Nanjing University, Nanjing 210093, P. R. China.
†These authors contributed equally to this work

References

1 F. Castet, V. Rodriguez, J.-L. Pozzo, L. Ducasse, A. l. Plaquet and B. Champagne, *Acc. Chem. Res.*, 2013, **46**, 2656-2665.
2 P. C. Ray, *Chem. Rev.*, 2010, **110**, 5332-5365.
3 H. Xu, R. Chen, Q. Sun, W. Lai, Q. Su, W. Huang and X. Liu, *Chem. Soc. Rev.*, 2014, **43**, 3259-3302.
4 R. Hu, N. L. Leung and B. Z. Tang, *Chem. Soc. Rev.*, 2014, **43**, 4494-4562.
5 G. S. He, L.-S. Tan, Q. Zheng and P. N. Prasad, *Chem. Rev.*, 2008, **108**, 1245-1330.
6 R. D. Wampler, A. J. Moad, C. W. Moad, R. Heiland and G. J. Simpson, *Acc. Chem. Res.*, 2007, **40**, 953-960.
7 S. Kawata and Y. Kawata, *Chem. Rev.*, 2000, **100**, 1777-1788.
8 J. Rotzler, *Tailoring Intra-and Intermolecular Properties: From Cyclophanes to Daisy Chains*, Verlag Dr. Hut, 2012, 119-126.
9 C. Ravikumar, I. H. Joe and V. Jayakumar, *Chem. Phys. Lett.*, 2008, **460**, 552-558.
10 I. D. Albert, T. J. Marks, and M. A. Ratner, *J. Am. Chem. Soc.*, 1998, **120**, 11174–11181.
11 S. Righetto, S. Rondena, D. Locatelli, D. Roberto, F. Tessore, R. Ugo, S. Quici, S. Roma, D. Korystov and V. I. Srdanov, *J. Mater. Chem.*, 2006, **16**, 1439-1444.
12 M. C. Ruiz Delgado, J. Casado, V. Hernandez, J. T. López Navarrete, J. Orduna, B. Villacampa, R. Alicante, J.-M. Raimundo, P. Blanchard and J. Roncali, *J. Phys. Chem. C*, 2008, **112**, 3109-3120.
13 A. Colombo, D. Locatelli, D. Roberto, F. Tessore, R. Ugo, M. Cavazzini, S. Quici, F. De Angelis, S. Fantacci, I. Ledoux-Rak, N. Tancrez and J. Zyss, *Dalton Trans.*, 2012, **41**, 6707-6714.
14 T. Schwich, M. P. Cifuentes, P. A. Gugger, M. Samoc and M. G. Humphrey, *Adv. Mater.*, 2011, **23**, 1433-1435.
15 R. L. Roberts, T. Schwich, T. C. Corkery, M. P. Cifuentes, K. A. Green, J. D. Farmer, P. J. Low, T. B. Marder, M. Samoc and M. G. Humphrey, *Adv. Mater.*, 2009, **21**, 2318-2322.
16 E. Cariati, M. Pizzotti, D. Roberto, F. Tessore and R. Ugo, *Coord. Chem. Rev.*, 2006, **250**, 1210-1233.
17 D. Espa, L. Pilia, L. Marchiò, M. Pizzotti, N. Robertson, F. Tessore, M. L. Mercuri, A. Serpe and P. Deplano, *Dalton Trans.*, 2012, **41**, 12106-12113.
18 K. A. Green, M. P. Cifuentes, M. Samoc and M. G. Humphrey, *Coord. Chem. Rev.*, 2011, **255**, 2530-2541.
19 J. C. Tan and A. K. Cheetham, *Chem. Soc. Rev.*, 2011, **40**, 1059-1080.
20 C. Guerrero-Sanchez, B. G. Lohmeijer, M. A. Meier and U. S. Schubert, *Macromolecules*, 2005, **38**, 10388-10396.
21 U. S. Schubert, A. Winter and G. R. Newkome, *Terpyridine-based materials: for catalytic, optoelectronic and life science applications*, John Wiley & Sons, 2011, 65-67.
22 F. Tessore, D. Roberto, R. Ugo, M. Pizzotti, S. Quici, M. Cavazzini, S. Bruni and F. De Angelis, *Inorg. Chem.*, 2005, **44**, 8967-8978.
23 X. Chen, Q. Zhou, Y. Cheng, Y. Geng, D. Ma, Z. Xie and L. Wang, *J. Lumin.*, 2007, **126**, 81-90.
24 Y. H. Lee, N. V. Nghia, M. J. Go, J. Lee, S. U. Lee and M. H. Lee, *Organometallics*, 2014, **33**, 753-762.
25 M. R. Harpham, O. z. n. Süzer, C.-Q. Ma, P. Bäuerle and T. Goodson III, *J. Am. Chem. Soc.*, 2009, **131**, 973-979.
26 C. R. Moylan, B. J. McNelis, L. C. Nathan, M. A. Marques, E. L. Hermstad and B. A. Brichler, *J. Org. Chem.*, 2004, **69**, 8239-8243.
27 V. PushkaraáRao, *J. Chem. Soc., Chem. Commun.*, 1993, 90-92.
28 S.-S. Sun, C. Zhang, L. R. Dalton, S. M. Garner, A. Chen and W. H. Steier, *Chem. Mater.*, 1996, **8**, 2539-2541.
29 A. Wojciechowski, M. M. M. Raposo, M. C. R. Castro, W. Kuznik, I. Fuks-Janczarek, M. Pokladko-Kowar and F. Bureš, *J. Mater. Sci. - Mater. Electron.*, 2014, **25**, 1745-1750.
30 I. F. Perepichka and D. F. Perepichka, *Handbook of thiophene-based materials: applications in organic electronics and photonics*, Wiley Online Library, 2009, 2-4.
31 F. Schlutter, A. Wild, A. Winter, M. D. Hager, A. Baumgaertel, C. Friebe and U. S. Schubert, *Macromolecules*, 2010, **43**, 2759-2771.
32 M. Schmittel, V. Kalsani, R. S. Kishore, H. Cölfen and J. W. Bats, *J. Am. Chem. Soc.*, 2005, **127**, 11544-11545.
33 G. M. Sheldrick, *University of Göttingen, Germany*, 1997, 1456.
34 M. Frisch, G. Trucks, H. Schlegel, G. Scuseria, M. Robb and J. Cheeseman, *Inc., Wallingford, CT*, 2004.
35 B. Liu, Q. Zhang, H. Ding, G. Hu, Y. Du, C. Wang, J. Wu, S. Li, H. Zhou and J. Yang, *Dyes Pigments*, 2012, **95**, 149-160.
36 G. R. Desiraju and T. Steiner, *Weak hydrogen Bond*, Oxford University Press New York, 2001, 6.
37 S. Bhowmik, B. N. Ghosh, V. Marjomäki and K. Rissanen, *J. Am. Chem. Soc.*, 2014, **136**, 5543-5546.
38 K. Nakamoto, *Infrared and Raman spectra of inorganic and coordination compounds. Part B., Applications in coordination, organometallic, and bioinorganic chemistry*, John Wiley, 2009, 23-25.
39 G. Wu, C. Norris, H. Stewart, H. Cox and A. J. Stace, *Chem. Commum.*, 2008, 4153-4155.
40 V. W.-W. Yam and K. M.-C. Wong, *Chem. Commum.*, 2011, 47, 11579-11592.
41 K. H. Y. Chan, J. W. Y. Lam, K. M. C. Wong, B. Z. Tang and V. W. W. Yam, *Chem. Eur. J.*, 2009, **15**, 2328-2334.
42 J. Shen, W.-D. Cheng, D.-S. Wu, Y.-Z. Lan, F.-F. Li, S.-P. Huang, H. Zhang and Y.-J. Gong, *J. Phys. Chem. A*, 2006, **110**, 10330-10335.
43 L. Kang, D. M. Ramo, Z. Lin, P. D. Bristowe, J. Qin and C. Chen, *J. Mater. Chem. C*, 2013, **1**, 7363-7370.
44 T. Chen, Z. Sun, X. Liu, J. Wang, Y. Zhou, C. Ji, S. Zhang, L. Li, Z.-N. Chen and J. Luo, *J. Mater. Chem. C*, 2014, **2**, 8723-8728.

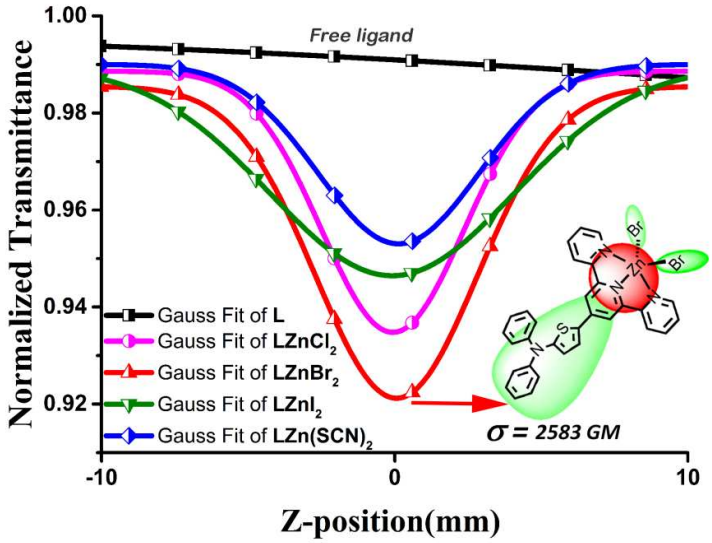

A thiophene-based terpyridine ligand (**L**) and its four zinc halide complexes (**$LZnCl_2$**, **$LZnBr_2$**, **$LZnI_2$** and **$LZn(SCN)_2$**) were synthesized and confirmed by single-crystal X-ray diffraction analysis. The open-aperture Z-scan results shown that **$LZnBr_2$** exhibit the best two-photon absorption property, which exceed free ligand **L** greatly.